Airborne surveys of snow depth over Arctic sea ice

R. Kwok,[1] B. Panzer,[2] C. Leuschen,[2] S. Pang,[1] T. Markus,[3] B. Holt,[1] and S. Gogineni[2]

Received 7 June 2011; revised 25 August 2011; accepted 26 August 2011; published 12 November 2011.

[1] During the spring of 2009, an ultrawideband microwave radar was deployed as part of Operation IceBridge to provide the first cross-basin surveys of snow thickness over Arctic sea ice. In this paper, we analyze data from three ~2000 km transects to examine detection issues, the limitations of the current instrument, and the regional variability of the retrieved snow depth. Snow depth is the vertical distance between the air-snow and snow-ice interfaces detected in the radar echograms. Under ideal conditions, the per echogram uncertainty in snow depth retrieval is ~4–5 cm. The finite range resolution of the radar (~5 cm) and the relative amplitude of backscatter from the two interfaces limit the direct retrieval of snow depths much below ~8 cm. Well-defined interfaces are observed over only relatively smooth surfaces within the radar footprint of ~6.5 m. Sampling is thus restricted to undeformed, level ice. In early April, mean snow depths are 28.5 ± 16.6 cm and 41.0 ± 22.2 cm over first-year and multiyear sea ice (MYI), respectively. Regionally, snow thickness is thinner and quite uniform over the large expanse of seasonal ice in the Beaufort Sea, and gets progressively thicker toward the MYI cover north of Ellesmere Island, Greenland, and the Fram Strait. Snow depth over MYI is comparable to that reported in the climatology by Warren et al. (1999). Ongoing improvements to the radar system and the utility of these snow depth measurements are discussed.

Citation: Kwok, R., B. Panzer, C. Leuschen, S. Pang, T. Markus, B. Holt, and S. Gogineni (2011), Airborne surveys of snow depth over Arctic sea ice, *J. Geophys. Res.*, *116*, C11018, doi:10.1029/2011JC007371.

1. Introduction

[2] The transfer of heat through the pack ice is regulated by ice thickness and by the thickness of the snow cover on the ice. Since snow is an effective barrier to heat transfer, the large-scale spatial distribution of snow depth and its small-scale variability associated with sea ice topography must be considered in any attempt to evaluate regional energy balance. However, snow depth observations are scarce. Measurements from field surveys [*Sturm et al.*, 2002, 2006] are restricted to understanding local variability. Using snow depth and density measured at Soviet drifting stations, *Warren et al.* [1999, hereinafter W99] provided the most comprehensive analysis of the snow depth of the Arctic Ocean currently available. However, this climatology was developed using data collected between 1954 and 1991; whether this compilation represents present-day snow conditions is not clear. Moreover, it is only representative of snow depth over relatively level multiyear sea ice, and it does not address the snow depth over the increasing expanse of seasonal ice in the Arctic. Additionally, the later onset of freeze and snow accumulation [*Markus et al.*, 2009] must have an impact on the interannual variability of total accumulation. From a remote sensing perspective, snow depth is a crucial parameter for the computation of snow loading in the freeboard-based estimation of sea ice thickness from lidar and radar altimetry [*Kwok and Cunningham*, 2008; *Giles et al.*, 2007].

[3] Because of the importance of snow depth in sea-ice mass balance and in the surface heat and energy budget, remote determination of snow depth at almost any spatial scale has long been desired. NASA's IceBridge mission offered an opportunity to demonstrate the capability to map snow depth from an aircraft. Operation IceBridge (OIB) was implemented as an airborne remote sensing program to extend the laser altimeter time series through the gap between the end of ICESat data collection in 2009 and the launch of the ICESat 2 lidar in the 2016. The primary goal is to minimize the impact of the interruption of the lidar time series established by ICESat for monitoring changes in the polar sea ice covers and ice sheets. An ultrawideband (UWB) radar for measuring snow depth was added to the IceBridge platforms (DC-8 and P-3) to allow demonstration of the radar's capability to conduct cross-basin mapping. This OIB snow radar is an improved version of earlier ground-based systems designed and built at CReSIS [*Wilyard*, 2006; *Panzer et al.*, 2010]. The ground-based radar (2–8 GHz bandwidth) was tested on Antarctic sea ice during the austral summer of 2003 [*Kanagaratnam et al.*, 2007]. Results show that snow depth can be estimated to an accuracy of about 3 cm. An early version of the radar was subsequently flight tested over Arctic sea ice during the spring of 2006 [*Cavalieri and Markus*, 2006; *Wilyard*, 2006]. This system was then modified and improved to enable routine operation from a fast-moving,

[1]Jet Propulsion Laboratory, California Institute of Technology, Pasadena, California, USA.
[2]Center for Remote Sensing of Ice Sheets, University of Kansas, Lawrence, Kansas, USA.
[3]NASA Goddard Space Flight Center, Greenbelt, Maryland, USA.

0148-0227/11/2011JC007371

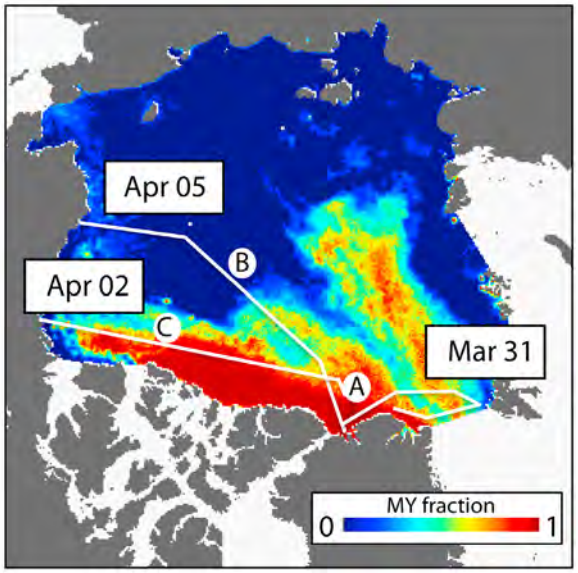

Figure 1. Tracks of three IceBridge flights (white) in Spring of 2009 over a map of multiyear sea ice coverage from QuikSCAT. Radar and lidar data acquired during these flights, each ~2000 km in length, are analyzed in this paper. Date flown is shown next to each track. Location of radar segments A, B, and C is shown in Figures 2, 3, and 4, respectively.

long-range aircraft on the IceBridge mission [*Patel*, 2009; *Panzer et al.*, 2010]. Analysis of the data acquired by this snow radar is the subject of this paper.

[4] The first Arctic deployment of the OIB airborne assets was in March and April of 2009. Data from three OIB flight lines, each covering ~2000 km in distance, are used in our analysis (Figure 1). These long transects were selected to provide a broad sampling of the snow and ice prior to the expected onset of melt over the Arctic sea ice cover. They were flown on 31 March, 2 April, and 5 April. Based at the Thule airbase, the first flight sampled the ice cover of the Lincoln Sea, north of the Greenland Coast, and the Fram Strait. The next flight, from Thule to Fairbanks, sampled the edge of the tongue of mixed multiyear/first-year sea ice west of the Canadian Arctic Archipelago. The return flight (5 April) flew north to 86°N, acquiring data over the large expanse of seasonal ice in the Beaufort Sea before turning east and collecting data over a patch of multiyear sea ice (MYI) and finally crossing the Greenland coast. These acquisitions represent the first trans-Arctic airborne surveys of snow depth over Arctic sea ice. All OIB flight lines have been designed, within the limits of the airborne platform and airspace restrictions, to sample the gradient in ice thickness across the Arctic Ocean. Some of these flight lines will be repeated annually throughout OIB.

[5] The paper is organized as follows. Section 2 describes the instruments and the data sets used in our analysis. In section 3, the following topics are addressed: (1) the phenomenology of radar backscatter from the snow cover; (2) our approach for identifying the air-snow and snow-ice interfaces in the radar echoes; and, (3) the estimation of snow depth and the uncertainties introduced by different error sources. The results from the three surveys are provided in section 4. The regional distribution of the snow depth estimates and their relationships to sea ice freeboard are examined. These estimates are then compared to climatology. Summary remarks and conclusions are provided in section 5. Section 3 deals primarily with remote sensing issues and may be skipped for readers interested in only the snow depth results.

2. Data Description

[6] Data sets from Operation IceBridge (OIB) are archived at the National Snow and Ice Data Center (NSIDC). Of the suite of OIB instruments, the two instruments of interest in this paper are the ultrawideband radar used for snow depth estimates (referred to as the snow radar) and the Airborne Topographic Mapper (ATM) used to provide high-precision lidar mapping of sea ice elevation. These instruments are operated simultaneously and provide coincident coverage, albeit at different spatial resolutions. In this section, we provide a brief description of the performance and coverage of the radar and lidar systems.

2.1. Snow Radar

[7] As mentioned earlier, a configuration of the snow radar adapted to the requirements of OIB was flown on the first Arctic campaign in the spring of 2009. Since that time the system has been deployed for annual mapping of snow depth over Arctic (spring 2010 and 2011) as well as Antarctic sea ice (austral spring 2009 and 2010). The exact system parameters, including pulse length and bandwidth, were optimized to meet specific flight parameters.

[8] The system is a nadir-looking radar that operates in a frequency-modulated, continuous-wave mode (FM-CW), and was designed and built by the Center for Remote Sensing of Ice Sheets (CReSIS) at the University of Kansas. Some relevant parameters of the snow radar are shown in Table 1. A bandwidth of 2.5–7 GHz combined with a sweep duration of 270 μs provides the fine range resolution (~5 cm in free space) needed to resolve the air-snow (a-s) and snow-ice (s-i) interfaces in the Arctic, where average snow depths are expected to be less than several tens of centimeters. The pulse repetition frequency controls the interval between subsequent transmitter chirps and thus the spatial separation between radar spots on the ground. As the radar is operated in real aperture mode, the aircraft altitude and speed determines the approximate spot size on the ground. At an altitude of ~500 m and a speed of ~250 kts (the nominal flight parameters for all OIB sea ice surveys), the ground track is sampled approximately every meter with a radar spot size of ~6.5 m. How is the spot size determined? Nadir radar returns from snow covered sea ice consist of coherent and incoherent components. When interface reflections from relatively smooth surfaces are clearly visible, the coherent term normally

Table 1. Characteristics of the University of Kansas Snow Radar

Radar Parameter	Setting
Bandwidth	2.5 to 7 GHz
Pulse Length	270 μs
Pulse Repetition Frequency	2 kHz
Transmit Power	20 dBm
IF Frequency Range	41–58 MHz
Sampling Frequency	58.32 MHz
Range Resolution (free space)	~5 cm

dominates. In such cases, the size of the footprint can be determined by the first Fresnel zone, where the radius of the spot is $8.657\sqrt{2d/f}$ (in meters). In the equation, d is the distance (in kilometer) to the surface and f is the highest frequency (in Ghz) of the radar's bandwidth. With $d = 0.5$ km and $f = 7$ Ghz, the diameter of the footprint is 6.5 m. The reader is referred to the published literature for a more detailed description of the radar system [*Kanagaratnam et al.*, 2007; *Wilyard*, 2006; *Patel*, 2009; B. Panzer et al., Development of an ultrawideband radar for measuring snow thickness on sea ice, in preparation for *Journal of Glaciology Instruments and Methods*, 2011]. The snow radar data are distributed to users in individual files each containing 4000 radar echograms that span ~4 km on the ground. Henceforth, we refer to these files as radar segments.

2.2. ATM Lidar

[9] The ATM is a conical-scanning laser ranging system operated at a wavelength of 532 nm with a pulse repetition frequency of 5 kHz and scan rate of 20 Hz with an off-nadir scan angle of 15° [*Krabill et al.*, 2002]. With the nominal OIB flight parameters described above (i.e., operating altitude and ground speed: 500 m and 250 kts), the ATM observation geometry provides an across-track scan swath of ~250 m with the laser illuminating a 1 m diameter footprint sampled approximately every 3–4 m along- and across-track near the center of the scan swath; the sampling becomes denser (submeter) near the edges of the swath because of conical scanning geometry of the system.

[10] The beam of the ATM generally backscatters sufficiently from a snow or ice surface to measure the time delay of a return signal and determine a total propagation distance. The presence of extremely smooth surfaces along the flight path resulted in some measurement dropouts, probably because of the forward scattering of the ATM beam. The travel time data are combined with GPS navigation measurements and aircraft orientation parameters to derive surface elevation measurements relative to the WGS84 reference ellipsoid, with a typical accuracy better than 10 cm [*Krabill et al.*, 2002]. The ATM elevations are provided in data files that cover tracks of ~35 km, each containing over a million elevation estimates.

2.3. Other Data Sets

[11] Basin-scale estimates of MYI coverage from April of 2009 are from analysis of QuikSCAT data (see Figure 1). Estimation and assessment of the spatial distribution of MYI coverage from scatterometer fields are described by *Kwok* [2004]. This data set is primarily used to understand the variability of snow depth over the two dominant ice types in the Arctic Ocean.

3. Data Analysis

[12] This section is divided into three parts. First, we discuss the radar phenomenology in the echograms. Then, the procedures used to detect the air-snow (a-s) and snow-ice (s-i) interfaces in the radar echoes are outlined. Finally, we describe how snow depths are estimated and the potential uncertainties associated with these estimates.

3.1. Radar Phenomenology

[13] Three radar/lidar composites (shown in Figures 2, 3 and 4) illustrate the mix of radar returns from multiyear and seasonal sea ice, and thin ice/open water. Each composite is constructed with data from coregistered segments (4 km) of ATM elevations and snow radar returns: individual elevation samples along the profile in Figure 2b are average elevations of ATM samples (~1 m) within the approximate spot covered by the snow radar (~3.5 m in radius); color-coded echograms (Figure 2c) show the magnitude of range-varying backscatter along track; and, echograms from different sections of the segment are shown in Figure 2d. Individual echograms show the range and the relative strength of the echo. The locations of these three segments are shown in Figure 1.

[14] The sample echo profiles in Figure 2d, from a relatively thick snow cover on multiyear sea ice, show that the a-s and s-i interfaces are well resolved. Here, we first discuss the terminology used to describe the features in the echograms (see Figure 5). In each echo profile, there is a distinct leading edge in response to the transition from the air to the snow volume. A local peak that is characteristic of the location of the a-s interface follows. The highest unambiguous peak in the profile is typically the return from the s-i interface. These two peaks represent quasi-specular reflections from the air-snow and snow-ice interfaces. Between the two peaks, there are often returns that may be indicative of scattering from internal layers within the snow volume as demonstrated with ground-based systems [*Kanagaratnam et al.*, 2007]. However, multiple layering is far more likely in Antarctic than in the Arctic. Past the trailing edge of the s-i peak, the radar trace does not return to the noise level that precedes the leading edge. These are off-nadir returns from the a-s interfaces and snow volume beyond the ranges of the s-i interface; the angular (or time) extent of these signals is determined by the backscatter response of the target as well as the antenna beam width.

[15] The color-coded echograms in Figure 2c also show that magnitude of s-i peaks (in red) are distinct from that of the snow surface. Under certain conditions, however, the returns from the snow/ice cover are nearly undetectable and appear as data gaps in Figure 2c. This seems to occur when the surface relief within the illuminated radar spot (~6.5 m) is highly variable, because of the mix of returns from surfaces at different ranges. Examination of the ATM elevation fields (Figure 2a) shows that this phenomenon seems to be associated with pressure ridges crisscrossing the radar track. Why are radar echoes from ridges nearly undetectable? If the pulse-to-pulse radar returns vary significantly or decorrelate over short distances, then coherent averaging of the returns (which is part of the data collection process) would reduce the signal in the data. At least this is what one expects to occur when there are sea ice ridges with base widths of only several meters (compared to ground sampling intervals of ~1.0 m) and with asymmetric snowdrifts with significant surface slopes relative to the horizontal. In these cases, a well-defined layer of snow over a flat ice surface does not exist and coherence is thus reduced. The absence of snow at the crests of pressure ridges is also a confounding effect. This blurring of the interfaces in the radar data warrants further investigation and is a potential limitation of the current radar implementation and processing methodology.

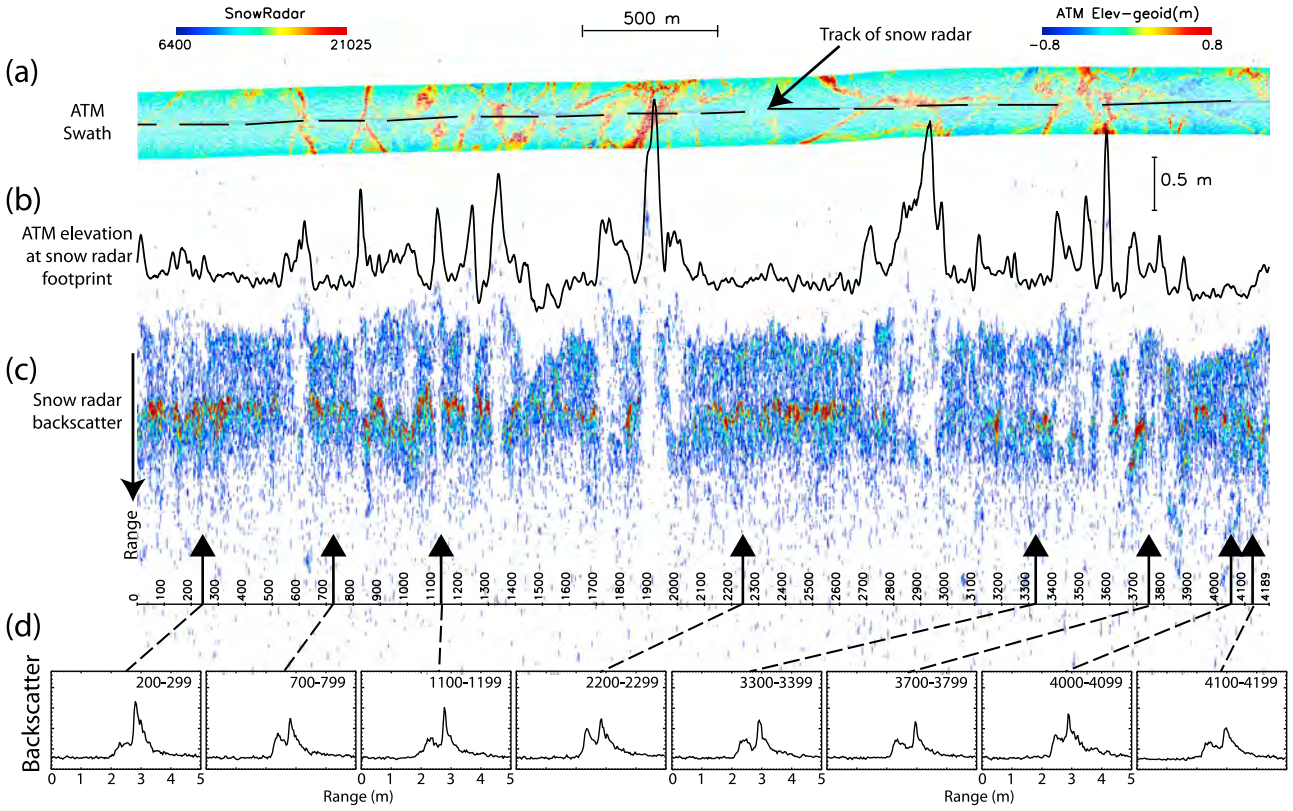

Figure 2. A 4 km segment of Airborne Topographic Mapper (ATM) lidar and snow radar data over thick multiyear ice from the 2 April IceBridge flight. (a) ~250 m ATM lidar swath with color-coded elevation. The track of the snow radar (black dashed line) is near the center of the lidar swath. (b) Average lidar elevation associated with each snow radar footprint of ~8 m in radius. (c) Range-varying backscatter along the track of the snow radar (high backscatter in red). Range direction is on the left side of the figure. (d) Sample backscatter profiles (average of 100 snow radar returns) from eight locations. Radar backscatter magnitudes are uncalibrated, so only the relative magnitudes are meaningful. Location of radar segment (A) is shown in Figure 1.

[16] Figure 3 shows the radar echoes from a thinner snow cover on seasonal ice in the Western Arctic (see location in Figure 1). In contrast to the profiles in Figure 2, the separations between the a-s and s-i peaks are lower. Even though the peaks are still distinct, this highlights the limits of the measurement system as the distance between the peaks approaches the range resolution of the radar system (discussed below).

[17] Returns from relatively smooth surfaces (possibly open water or very thin ice) are shown in the radar segment in Figure 4. In the sample echo profiles in Figure 4d, there are no observable a-s transitions in the returns from these snow-free surfaces. In fact, a trailing peak, a characteristic of the impulse response of this radar system (i.e., sidelobe), following the main peak of the surface return (~15 cm downrange) is apparent. These downrange sidelobes are not visible in the echograms in Figure 2d because of the lower returns from the rougher s-i interface and because the radar clutter discussed above are higher than levels of the sidelobes. Since this sidelobe is on the trailing edge of the impulse response, it does not interfere with the detection of the a-s interface.

[18] The nearly pure surface returns seen in the 4 km segment in Figure 4 are also useful for providing a more quantitative assessment of the radar's range resolution and the expected level of the system sidelobes. We selected an echogram with the highest peak within the radar segment to examine the system characteristics. The analyzed results (in Figure 6) show that system response is asymmetric in range with a trailing edge sidelobe (discussed above) that is 8 dB below the peak of the main lobe; the leading edge side lobe is nearly 20 dB below the main lobe. The range resolution of the system, typically defined as the width of the main lobe at 3 dB below the peak, is ~4.9 cm, approximately the expected performance of the radar in Table 1. A cautionary note is that while the width of the main lobe is a measure of range resolution, it is useful only when the return levels of the two interfaces are comparable. If the scattering from the s-i interface is much stronger than that from the a-s interface, then the detectability of the weaker return could be masked by the main lobe of the higher s-i return, especially if the separation between the interfaces is small. The sidelobes seen here have been reduced in the 2010 deployment of the snow radar; the goal in system performance is to obtain sidelobes that are 40–50 dB below the main peak.

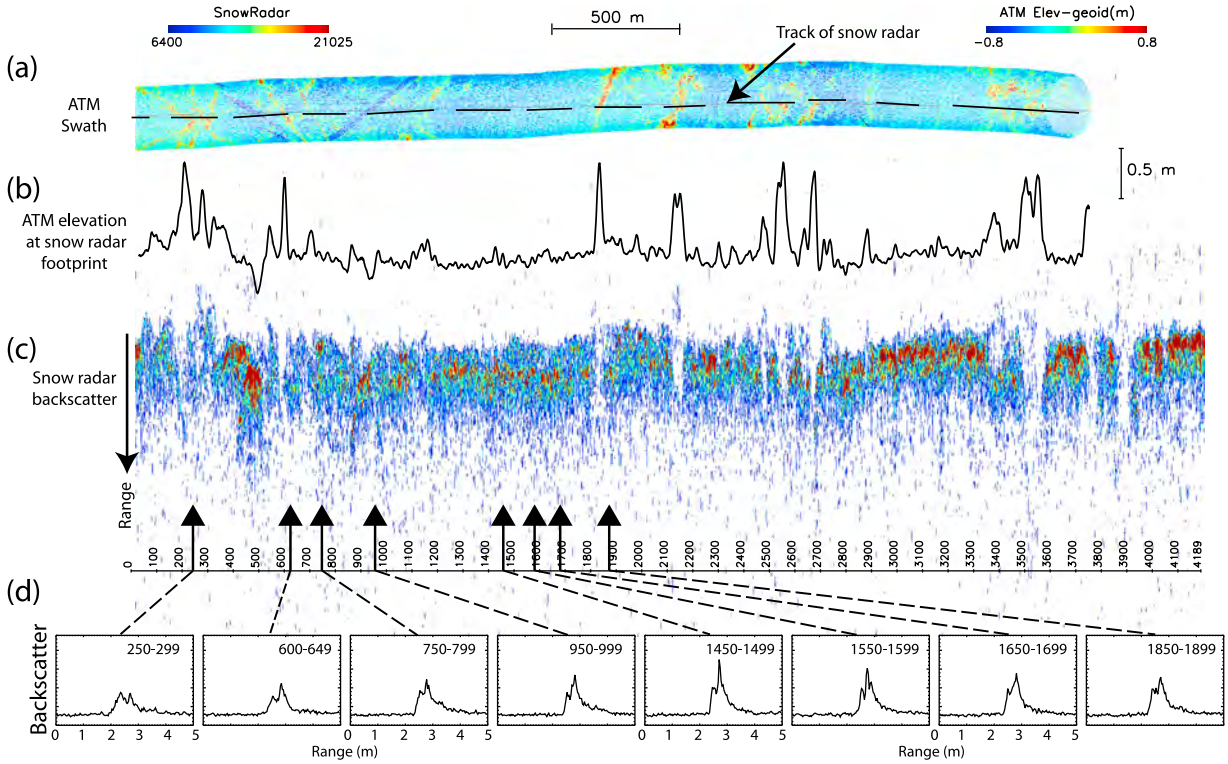

Figure 3. Snow radar response over seasonal ice from the 5 April IceBridge flight. For description, see caption in Figure 2. Sample backscatter profiles in Figure 3d are averages of 50 snow radar echograms. Location of radar segment (B) is shown in Figure 1.

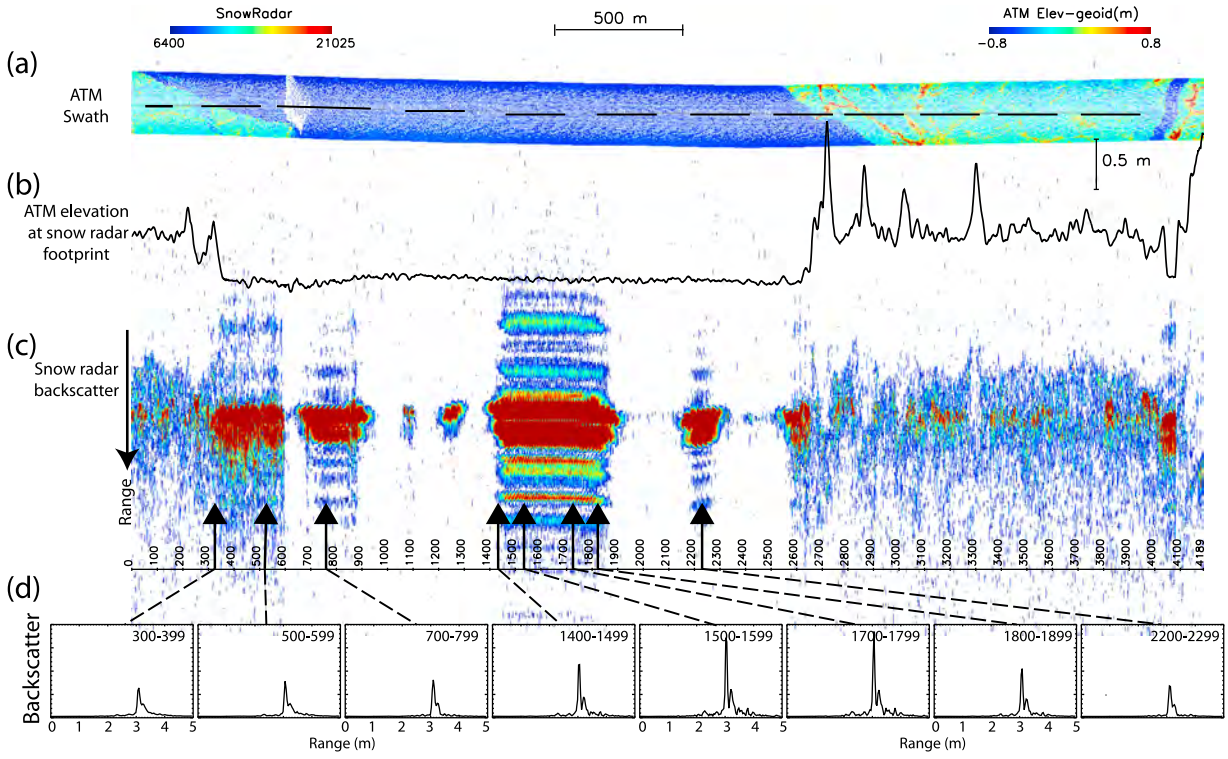

Figure 4. Snow radar response over thin ice/open water from the 2 April IceBridge flight. For description, see Figure 2 caption. Sample backscatter profiles in Figure 4d are averages of 100 snow radar echograms. Location of radar segment (C) is shown in Figure 1.

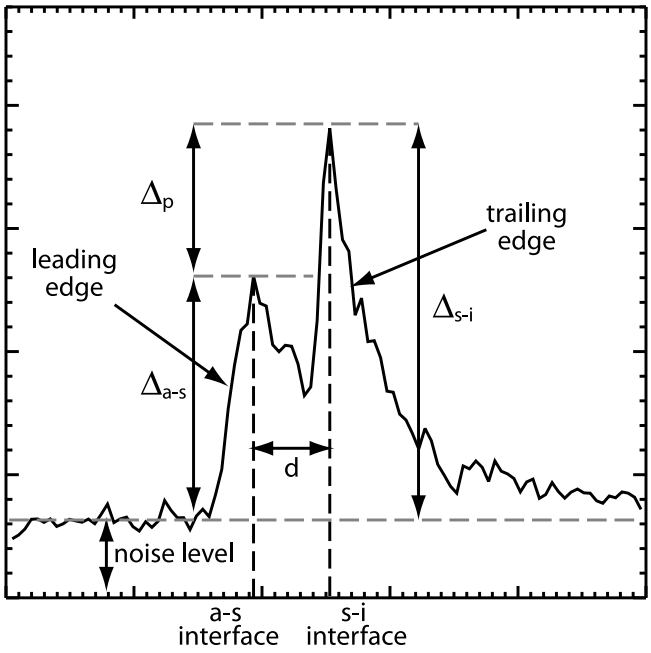

Figure 5. Terminology used to describe features in the radar echograms.

[19] The discussion has been rather qualitative thus far. The quantification of these parameters in the following discussion will inform the design of the procedures for retrieving the a-s and s-i interfaces, understanding the limitations of the measurement system, and estimating snow depth. Figure 5 summarizes the parameters and terminology that are of interest throughout this paper. The discussion has been rather qualitative thus far.

3.2. Detection of the Air-Snow and Snow-Ice Interfaces

[20] First, we describe the procedure used to detect the location of the a-s and s-i interfaces in individual echograms. Second, we describe the rationale and assumptions for each step and our choice of the controlling parameters. Since the exact operating radar parameters (including pulse lengths, bandwidths, and transmit power) are optimized to meet specific flight requirements, the thresholds specified below should be adapted to the settings of individual flights. The parameters below represent those selected for the flights of 2 April and 5 April.

[21] The steps in the procedure are described below. For each echogram:

[22] 1. Estimate the system noise level. The magnitude of the first 40 range samples in the echo profile is used to estimate the mean (m_n) and standard deviation (σ_n) of the system noise.

[23] 2. Identify the location of the s-i interface. The highest peak in the profile that is >6.0 dB above the mean noise level (m_n) of the system is designated as the s-i peak.

[24] 3. Locate the a-s transition. The leading edge is defined as the first occurrence of a forward difference (between the magnitudes of the range samples) greater than $3\sigma_n$. In addition, that location must be at least 4 range samples (free space range distance of ~13 cm) away from the location of the s-i peak. If the leading edge does not satisfy these conditions, an estimate of the location of a-s transition is not made for that radar profile.

[25] 4. Determine the location of the a-s peak and refine the location of the s-i peak. The echogram is oversampled by a factor of 4 (resulting in sample spacing of less than 1 cm). The first distinct peak after the a-s transition is designated as the location of the a-s interface. That peak has to be $>1\sigma_n$ above that of the adjacent samples. Similarly, the initial coarse location of the s-i peak is used as an estimate to refine the location of this interface.

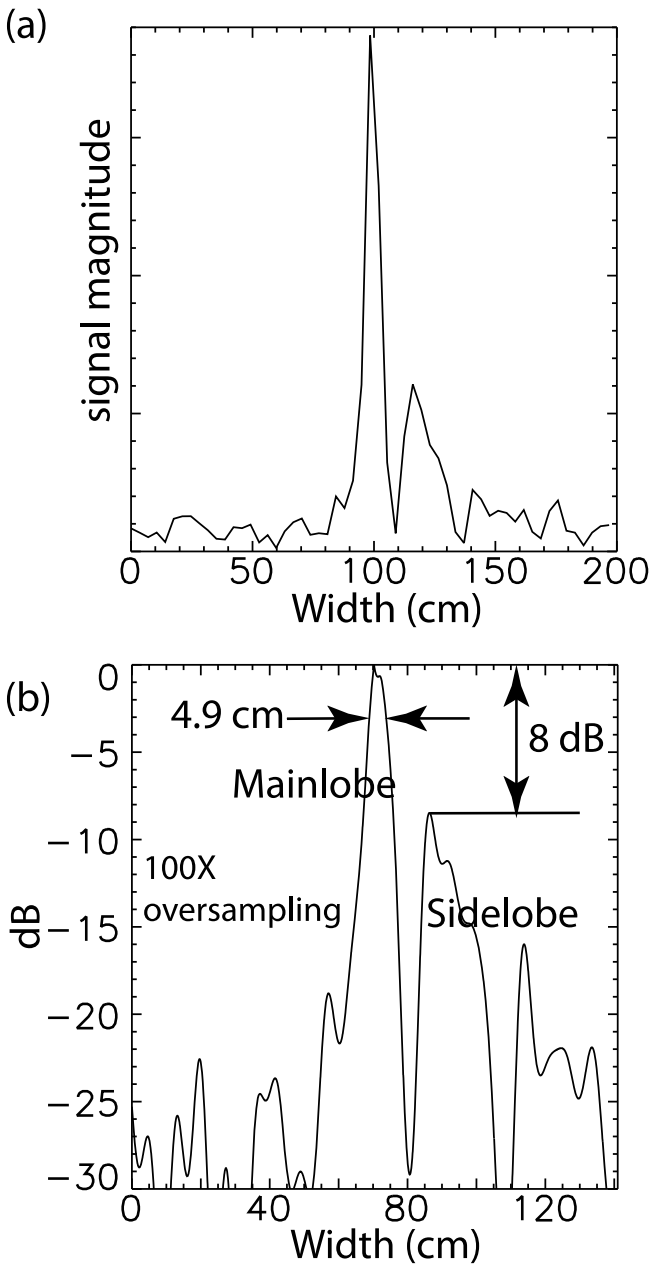

Figure 6. Radar echogram from a quasi-specular surface (very smooth surface) in Figure 3. (a) Magnitude. (b) Range resolution of the snow radar estimated as the width of the echo at 3 dB below the level of the peak.

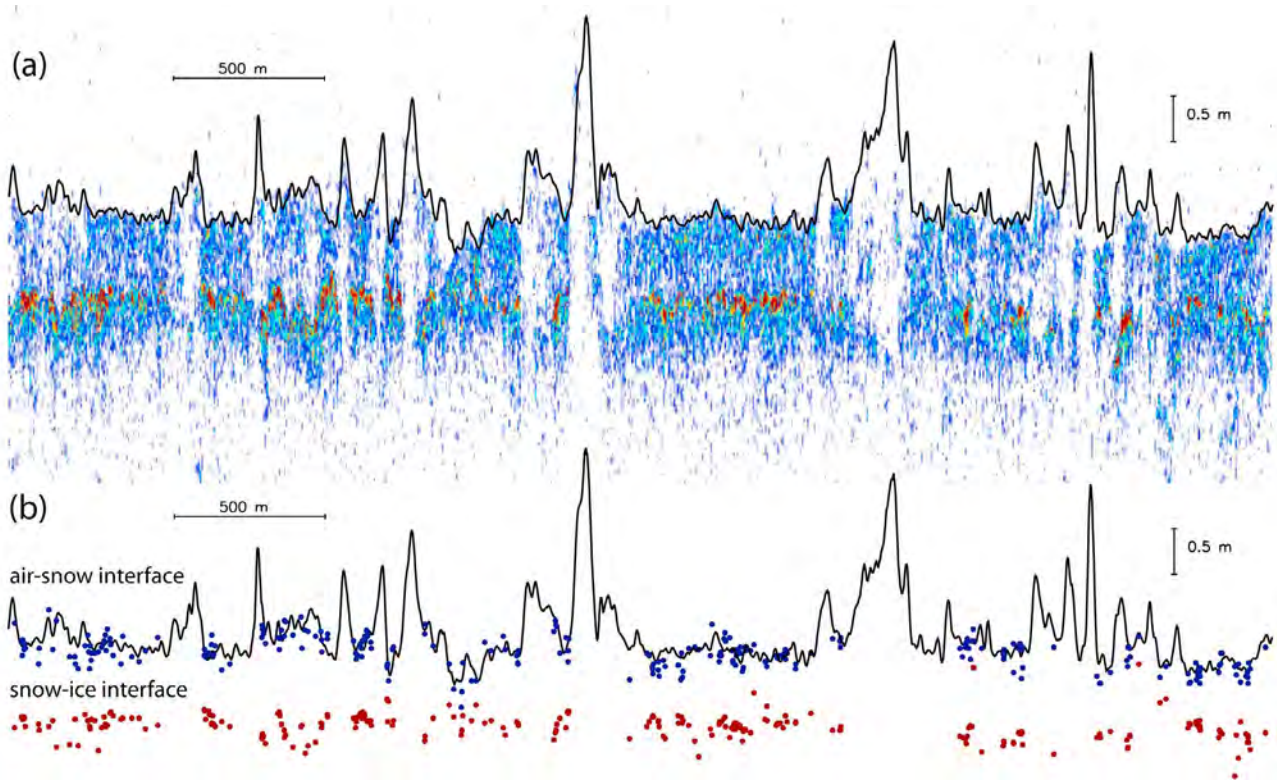

Figure 7. Alignment of air-snow interfaces from the ATM lidar and snow radar data (4 km segment from Figure 2). (a) Lidar profile and estimated location of air-snow interfaces in snow radar echoes. (b) Detected location of air-snow and snow-ice interfaces from procedure described in the text.

[26] Using the estimates from all echograms within each 4 km segment:

[27] 5. Register the along-track profile of the a-s interface to the ATM elevation profile (another estimate of the location of the a-s interface). This involves matching the mean elevations of the two profiles (see Figure 7).

[28] 6. Filter to remove outliers. After matching the mean levels, compute the elevation differences (σ –standard deviation) between the ATM surface and radar a-s interface. Deviations of a-s interface estimates that are greater than 2σ from that ATM surface are discarded. This step is repeated once after the initial removal of the outliers. The remaining samples are considered to contain the detected range locations of the a-s and s-i interfaces (Figure 7b).

[29] In the second step, the highest peak (>6 dB above the system noise) in the echogram is assumed to be the scattering from the s-i interface. We base this threshold on examinations of the average statistics of the echograms in the ~500 radar segments from each day. This step establishes a reference point from which to locate the a-s interface. We also identify a zone within which the radar response of the s-i interface is expected to interfere with the detection of the a-s interface; this is used in the following step. Figure 8 shows the distributions of the s-i peaks and the relative levels of the a-s and s-i peaks found by our procedure. For the two flights in April, the s-i peaks and a-s peaks are on average 7.5 dB and 5.0 dB above the noise floor. We find that these ratios are remarkably consistent and likely constrained by the thresholds used by our detection scheme. On average, the s-i peaks are >2.5 dB above the level of the a-s peaks. Potentially, the leading edge of the distributions suggests that the s-i peaks could be lower than the a-s peak, although this is not allowed by our procedure. These parameters are generally higher on the 31 March flight because the system parameters were set differently that day. In fact, the system seems to have performed better during that first flight perhaps because the snow cover is thickest.

[30] The next step finds the transition from air to snow. A distinct edge may be expected if the dielectric contrast at the interface is high, but this may not be true where there is fresh low-density snow over an older layer, or when the surface relief is such that the elevations of the a-s interfaces are highly variable over the radar footprint. In these cases, we expect the radar returns to be smeared and to become problematic in the detection process. Here, we delineate the leading edge as that location where the change in backscatter between successive radar samples is greater than three times the standard deviation of the system noise ($3\sigma_n$) calculated in the first step. If such a transition is found, we select this as the transition of the a-s interface. The procedure does not produce an estimate for a radar profile when these conditions are not satisfied. After finding the leading edge, we designate the first peak in the neighborhood of the transition to be the location of the a-s interface. This ensures that this peak is associated with the a-s interface. The locations of the two peaks are refined in the oversampled echo profile.

[31] In the last step, we compare the estimated elevations of all the a-s interfaces to the ATM surface profile to filter the outliers in our estimates (see Figure 7). To do so, the two a-s profiles (from the ATM and the snow radar) are first aligned

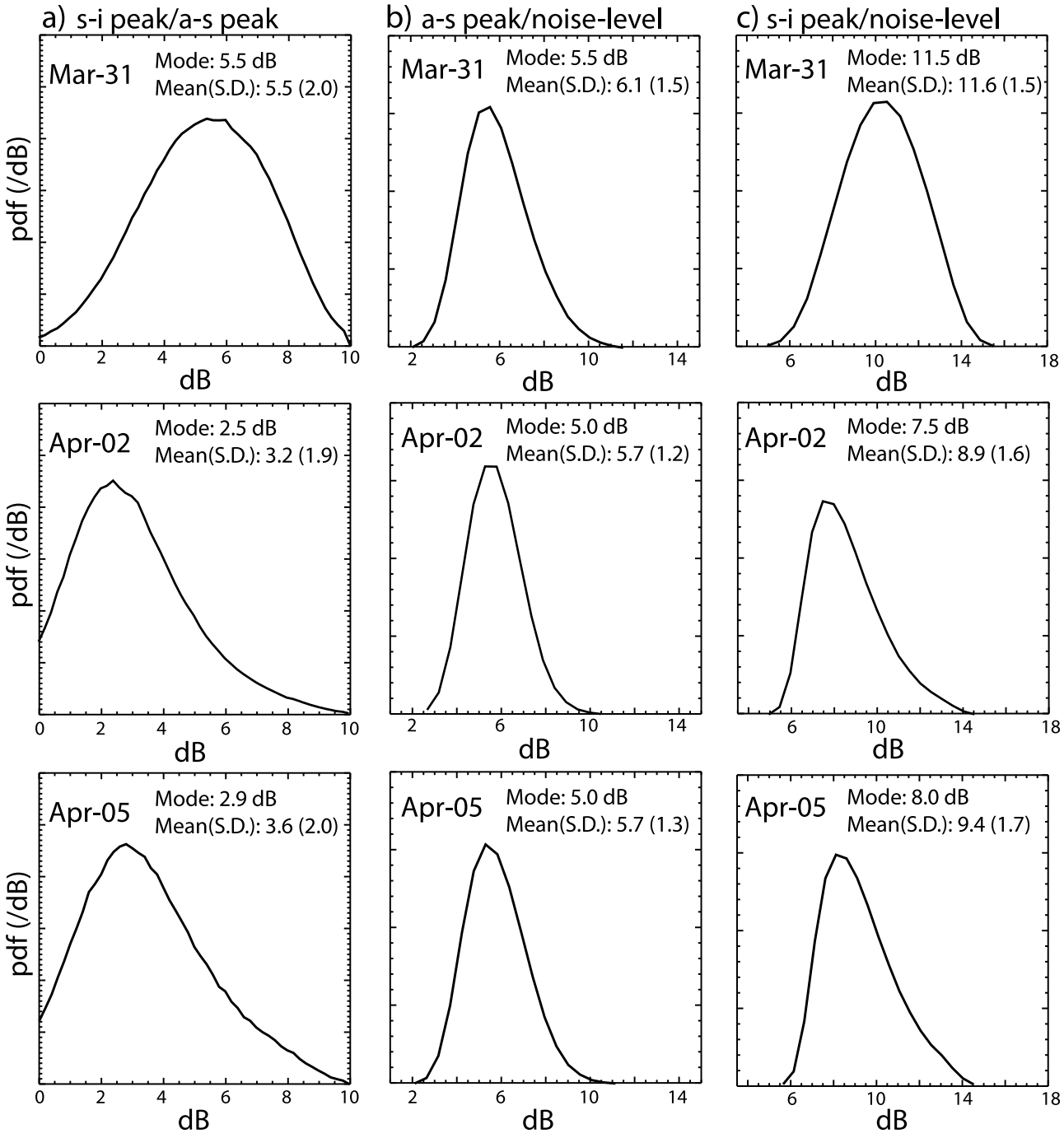

Figure 8. Relative magnitude of the air-snow interface, the snow-ice interface, and the noise level for the three surveys. (a) Ratio of the peak of the snow-ice and air-snow interfaces in the radar echogram (in dB). (b) Ratio of the air-snow peak and the noise level. (c) Ratio of the snow-ice peak and the noise level.

by removing the mean elevation differences between them. Deviations of a-s interface estimates that are greater than 2σ from that of the ATM surface are discarded. Because the scattering of the a-s interface is relatively weak and the peaks are less distinct (under conditions described above), we consider this step useful in removing the outliers from the retrievals.

[32] We consider this to be a rather conservative approach. Ensuring that the detected transition is significantly above the noise level reduces the false alarm rate. In consequence, we may miss smaller transitions that may be real. We will return to this discussion in the conclusion.

3.3. Retrieval of Snow Depth

[33] The vertical distance between the detected a-s and s-i interfaces is defined as the retrieved snow depth. However, the distances in the data are given in radar ranges (r) without correction for the speed of propagation in the snow volume. To compute the actual thickness of the snow layer between the two interfaces, we have to account for the

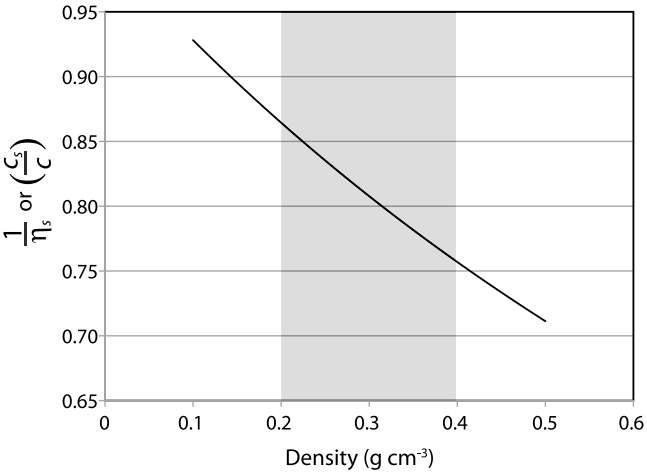

Figure 9. Dependence of speed of light or refractive index η_s on the density of dry snow. Gray region shows the range of densities of interest in this paper.

refractive index of the medium (snow). Assuming that the refractive index is uniform throughout the layer, the snow depth (d_s) can be written as:

$$d_s = \frac{(r_{as} - r_{si})}{\eta_s} = (r_{as} - r_{si})\frac{c_s}{c} \quad (1)$$

where r_{as} and r_{si} are the range distances to the a-s and s-i interfaces, η_s is the refractive index of the snow volume, and c_s is the speed of light in snow. In turn, η_s is dependent on the density of the dry snow. Following the approximation given by *Ulaby et al.* [1986]:

$$\eta_s = \sqrt{\varepsilon_r} = (1 + 0.51\rho_s)^{3/2}. \quad (2)$$

[34] In this equation, ε_r and ρ_s represent the real part of the dielectric constant and the density of the snow volume, respectively. The relationship between the fractional changes in the speed of light and the bulk density of the snow layer is plotted in Figure 9.

[35] According to the snow climatology of W99, the mean snow density varies seasonally and is ~0.3 ± 0.1 g/cm^3 in April. At a density of 0.3 g/cm^3, the propagation speed is ~0.81 times the speed of light in free space. Varying the density by 0.1 g/cm^3 changes the speed of propagation by ~5% (gray region in Figure 9). Consequently, the estimated depth is not particularly sensitive to variations in snow density, especially if equation (2) is used to represent the refractive index of the volume. More often than not, there are inhomogeneities (e.g., internal layers, density variations, etc.) that could introduce uncertainties into the snow depth estimate. In our conversion to snow depth, the variability in snow depth estimates due to these factors are not considered.

3.4. A Simple Error Analysis

[36] We offer an analysis of the lower bound in the uncertainties of the overall snow depth estimation process by considering only two error sources: range resolution and the variability in bulk snow density. For these two parameters, we assume that (1) there is a range resolution of ~5 cm (in free space) and the peaks of the a-s and s-i interfaces in the radar profile can be located to within ~3 cm (σ_i, approximately half the range resolution), and (2) the uncertainty in snow density is 0.1 g/cm^3. For a given radar profile, the uncertainty in snow depth, σ_s, can be written as,

$$\sigma_s^2 = m_c^2(2\sigma_r^2) + d_r^2\sigma_c^2.$$

σ_r is the uncertainty in the range locations of the interfaces; m_c and σ_c are the mean and uncertainty in the adjustments to the speed of propagation due to the uncertainties in the bulk density of dry snow, respectively.

[37] Assuming a nominal density of 0.3 g/cm^3 and σ_c = 0.05, the uncertainty in the snow depth estimate varies from ~3.5 cm to 5 cm for snow depths between 10 cm and 70 cm. In an ideal scenario, the interfaces would be step edges and the peaks would be of comparable magnitude. However, detection of the interfaces is affected by each of the previously mentioned factors. A more realistic analysis should include the expected variability of the interfaces within the radar footprint. Even though the peak in the s-i interface is distinct, this is not always the case for the a-s interface and thus typically there is higher uncertainty in its location.

[38] Because of the finite range resolution, there is also a limit below which snow depth retrieval would be difficult. Snow depth below a range resolution of 5 cm is difficult to resolve. This limit is further degraded if the scattering from the two interfaces was at different levels. Again, the stronger peak could mask the response of the weaker peak. Our detection procedure seldom provides snow depths that are below ~8 cm. Thus, the range resolution is an important parameter if shallower depths are of interest.

4. Results

[39] In this section, we discuss separately the snow depth estimates from the individual flights, their combined distributions over first-year and MYI, and comparisons with the climatology of W99. The snow depth estimates from the three flights (flown on 31 March, 2 April, and 5 April) are summarized in Figures 10, 11, and 12. The distance flown each day averages ~2000 km; we divide each track into four flight segments of ~500 km in length to show the regional variability and consistency in retrieval. In each of the summary figures, we show (1) the length of the four segments and the flight track on a map, (2) the estimated snow depth along each flight track, and (3) the snow depth distributions of the individual ~500 km flight segment. Table 2 summarizes the regional differences in the number of snow thickness retrievals (in percentages) from each flight and from each segment.

4.1. Snow Depth Estimates: 31 March

[40] This flight line acquired data over thick snow on the MYI cover of the Lincoln Sea, the sea ice north of the margins of Greenland, the Fram Strait, and the coast of Greenland (Figure 1). The along-track statistics (mean and standard deviation) of snow depth (in Figure 10b) are from the population of retrieved estimates within each 4 km radar segment. The size of these populations vary in size and depend on the detectability/quality of the a-s and s-i interfaces using the retrieval tool described in section 3. Thus, snow depth

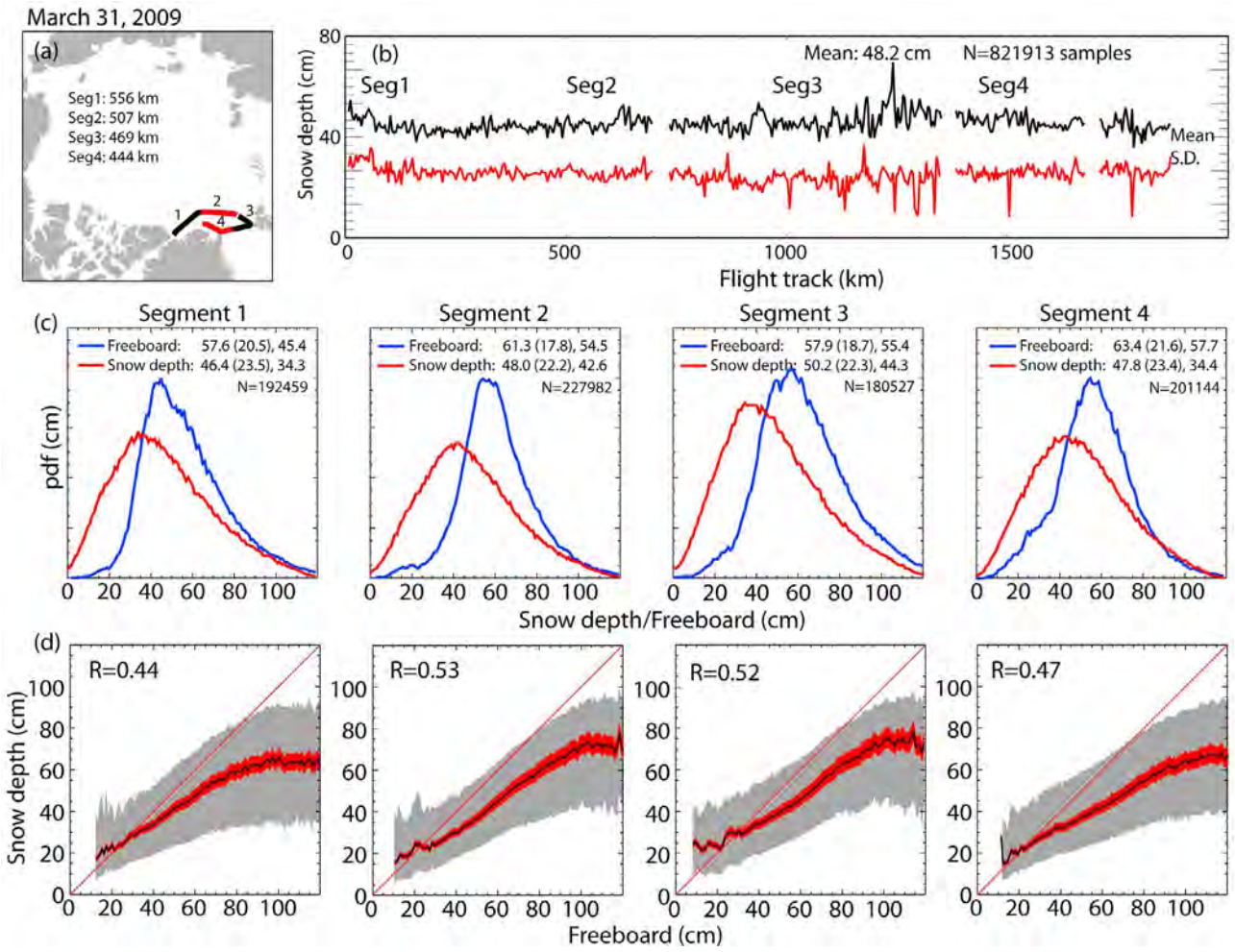

Figure 10. Snow depth and total freeboard (snow + ice) from the 31 March survey. (a) Track/segment length and location. Tracks are divided into four flight segments for examination of regional statistics. (b) Mean and standard deviation of snow depth along the track. The statistical moments are from the population of retrieved snow depth within a 4 km segment. (c) Distributions of snow depth and total freeboard within each flight segment. (d) Relationship between snow depth and total freeboard within each segment: the gray band shows the ±RMS excursions within a 1 cm bin, and the red band shows the variability associated with an uncertainty in snow density of ±0.1 g/cm^3. R is the correlation coefficient between snow depth and total freeboard.

estimates are available for only a fraction of each 4 km radar segment. Along this flight track, there are 821,913 retrievals in a total of 1.8 million echograms, or ~46% of the echograms (Table 2). Variability in the retrievals for the four segments is small. Retrievals are not available where the a-s interfaces are weak, there is open water, and the snow depths are shallow. It should also be noted that the number of retrievals is highly dependent on the detection algorithm and controlled by acceptable levels of detection errors. Here, the thresholds have been adjusted to use only distinct a-s transitions. At this time, an overall strategy to optimize the number of retrievals is not clear but future adjustments should include a better understanding of the expected scattering characteristics from the a-s interface.

[41] To better quantify the sensitivity of this combination of radar instrumentation and detection algorithms to surface relief, we contrast the standard deviations of the ATM elevation at the radar footprints where we have retrievals with those of the entire 4 km segment. We find (in Figure 13) that the standard deviations of the ATM elevations of the sample populations with retrievals are consistently lower than those of entire radar segments. Whereas the average standard deviation over the 4 km segments is 26.5 cm, the average is only 17.6 cm over those footprints with detected interfaces. This suggests that the subset of retrieved snow depth is generally over smoother, more level surfaces. The results from all three flights agree. These limitations of the retrievals that should be noted in the interpretation of the results that follow. Nevertheless, snow thickness on level ice may be an important snow variable because the modal snow thickness most likely coincides with the modal ice thickness, and largely determines how much freezing there is over level ice.

[42] Over the 31 March track, the mean snow depth is 48 cm with an overall standard deviation of ~30 cm. Figures 10c and 10d show the distributions of snow depth

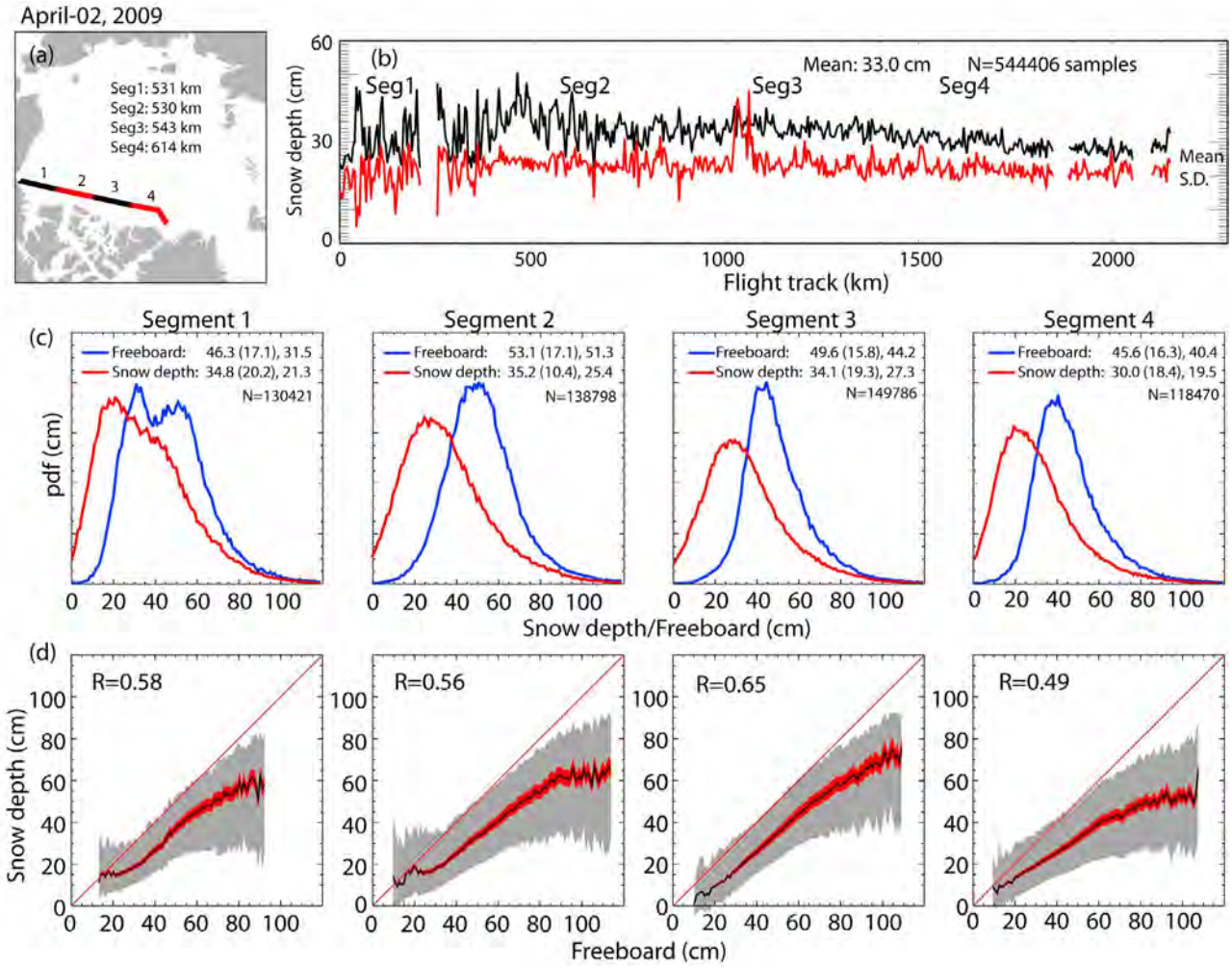

Figure 11. Snow depth and total freeboard from the 2 April survey. For description, see Figure 9 caption.

and total freeboard (i.e., snow + ice freeboard) for individual flight segments, and the relationship between the two quantities. Total freeboard (henceforth referred to as freeboard) is derived from the ATM lidar. The snow depth distributions are generally more skewed when compared to the more symmetric freeboard distributions. We expected the actual freeboard distributions to have longer tails [*Kwok et al.*, 2009], but this shape may again be due to the selective retrievals over level ice as discussed above.

[43] The thickest snow estimates (mean: 50 cm) is found in the acquisitions over Fram Strait (Segment 3). The modal snow depth in this segment is also higher than those in adjacent segments. In fact, this can be compared to the climatology shown in Figure 14b. This region has the thickest snow cover in the Arctic Ocean because it is in the path of storm tracks entering the Arctic Ocean from the Greenland Sea, and thus higher regional accumulation from precipitation. Distributions show retrievals that are over a meter and suggest that the snow radar is not limited by snow depth but rather by surface relief.

[44] The relationship between freeboard and snow depth (in Figure 10d) shows the fraction of the total freeboard (snow + ice) that is snow. Since negative freeboards are unlikely in the Arctic Ocean, all snow depths should be lower than the estimated freeboard (or, below the red line with unity slope in Figure 10d). In our measurements, however, noise contributes to the freeboard as well as the snow depth estimates. When the signal-to-noise level is low, or when the freeboards and snow depths are comparable, the incompatibility between freeboard and snow depth becomes more pronounced. For this flight, the incompatibility between these two parameters (i.e., snow depth > freeboard) is especially noticeable below 20 cm, but is less so in the results from the other two flights. Since these parameters are measured independently, systematic biases in the freeboard and snow depth estimates would shift these curves horizontally and vertically without changing the slope. It should be noted that at the leading and trailing edges of these distributions, the size of the population that constitutes these statistics is also quite small. We should also remember that the assumptions of bulk density might introduce variability in retrievals that is not well understood.

[45] These relationships are interesting. Not surprisingly, the spread of the data (gray region, Figure 10d) indicates that the variability in snow depth for a given freeboard is high. Correlations between the two parameters are between 0.44

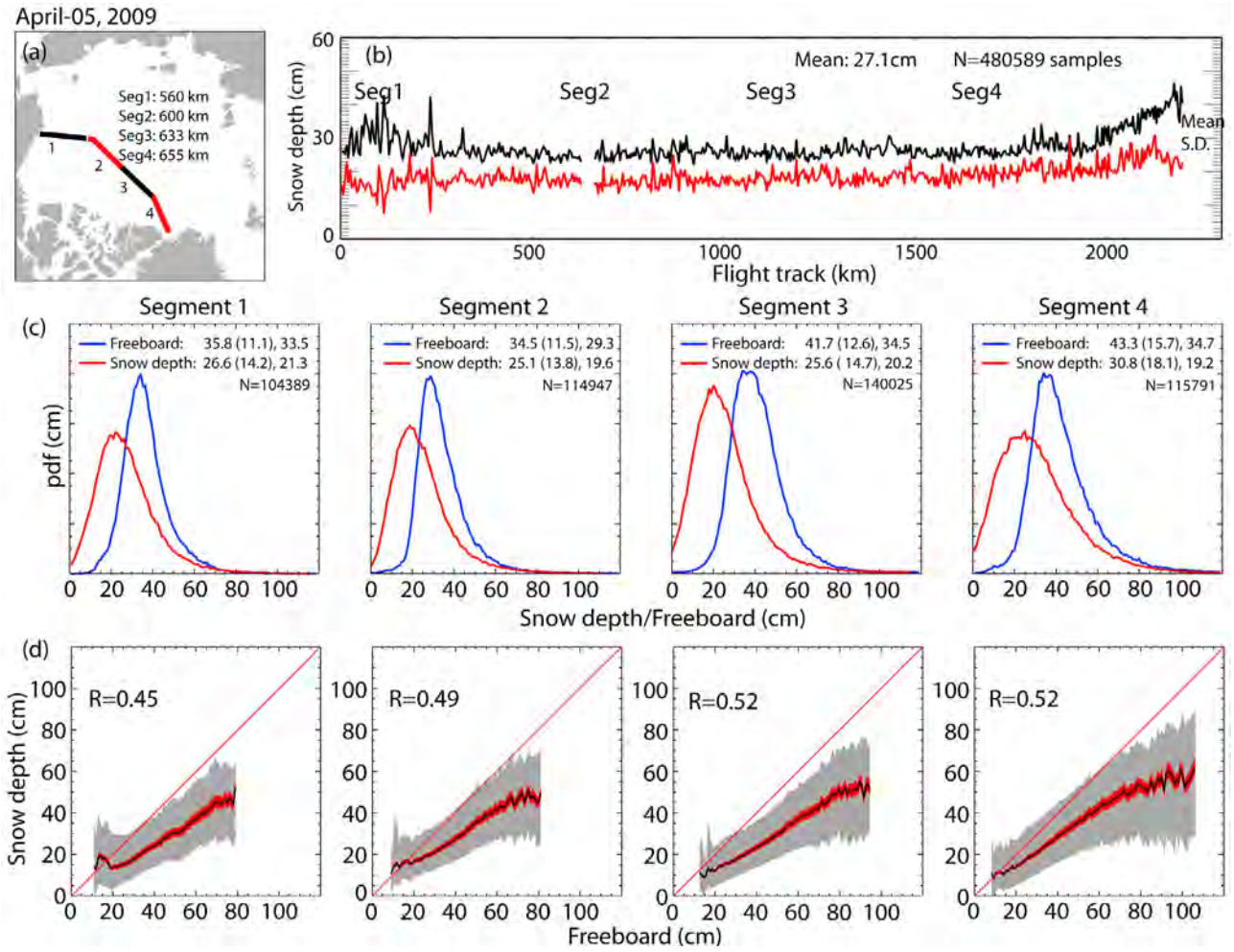

Figure 12. Snow depth and total freeboard from the 5 April survey. For description, see Figure 9 caption.

and 0.53. This suggests that at the scale of the radar footprint, freeboard is a poor but not totally unskilled predictor of snow depth. The fraction of the freeboard occupied by snow is highest in Segment 3 and lowest in Segment 4, i.e., the slope is steepest or closest to the line with unity slope.

[46] Another feature seen in Figure 10d is that the mean snow depth levels off at a certain freeboard beyond which changes in snow depth becomes negligible. Differences in this level in the four segments suggest a regional dependence. A likely cause of this plateau is that the net regional precipitation and accumulation over the season limit the snow depth over relatively level ice. Again, possibly because of the location of Segment 3, that fraction of the freeboard occupied by snow and that plateau in snow depth is higher because of precipitation due to storms from the Greenland Sea.

4.2. Snow Depth Estimates: 2 April

[47] The southern endpoint of this track is just north of the MacKenzie Delta (see Figure 1). The acquisitions are over a mix of seasonal and older ice near the edge of the MYI pack west of the Canadian Arctic Archipelago. The northern part of the track terminates just south of 86°N before it enters the thick MYI cover of the Lincoln Sea.

[48] Along this flight track, snow thickness estimates are obtained in ~37% of the radar echoes (Table 2). The mean snow thickness of 33 ± 25 cm (standard deviation of 18 cm) is thinner than that 44 ± 22 cm observed on the 31 March flight. The along-track profile (in Figure 11b) shows large variability in snow depth in Segment 1 and the early part in Segment 2, possibly due to the mixture of seasonal and old ice as evidenced by the bimodal character of the distributions in Figure 11c. As well, the snow depth climatology (in Figure 14b) also shows higher mean snow depth east of the Amundsen Gulf. However, this variability decreases significantly further north in Segments 3 and 4. The last part of Segment 4 shows an uptrend in snow thickness as the flight enters the thicker, older ice cover. This gradient is clearly seen in the profile of the following flight. Other than the features noted here, the distributions of snow depth and freeboard of the individual flight segments (Figure 11d) do not show

Table 2. Number of Snow Depth Estimates From Each Flight Segment (in Percent)[a]

	Segment 1	Segment 2	Segment 3	Segment 4	Overall
31 Mar	45.3	49.5	46.2	44.2	46.1
2 Apr	33.4	37.0	47.7	30.2	37.2
5 Apr	23.8	22.8	27.0	24.0	24.4

[a]Each segment contains approximately 450,000 echograms.

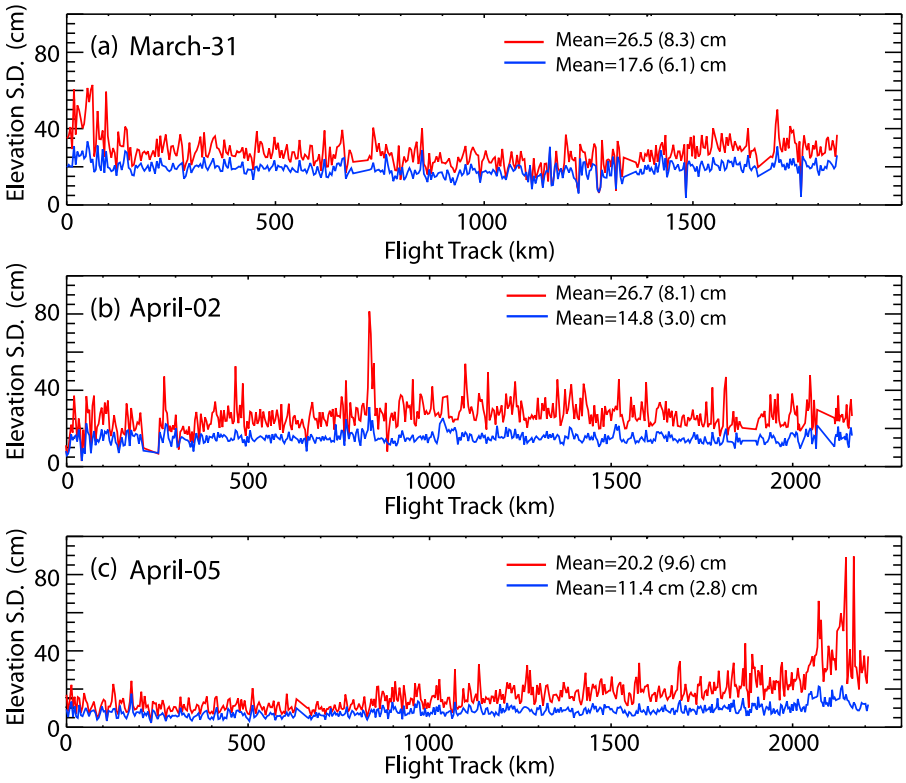

Figure 13. Surface roughness (standard deviation of surface elevation from the ATM lidar) at points with snow depth estimates (blue) compared to those over an entire 4 km radar segment (red).

differences that are remarkable. Also observed here is that the freeboard distributions are exceptionally symmetric, reinforcing our previous discussion of the sampling biases of the radar/detection system.

[49] The relationship between snow depth and freeboard is shown in Figure 11d. Correlations between the two parameters, between 0.49 and 0.65, are higher than those obtained from the estimates above (31 March). The plots show that snow depth and freeboard are largely compatible, i.e., freeboard > snow depth. All segments show the characteristic plateaus in snow depth seen on 31 March.

4.3. Snow Depth Estimates: 5 April

[50] This trans-Arctic survey originated east of Barrow and covered the large expanse of the seasonal ice in the Beaufort Sea and the Canada Basin (Figure 1). The flight also acquired data over the thick MYI cover just north of the Greenland coast prior to landing in Thule. This flight provided the best along-track profile for examining the gradient in Arctic snow depth in the regional transition from a purely seasonal to MYI cover.

[51] The along-track snow depth profile (in Figure 12b), with a mean thickness of 27 ± 20 cm, shows the thinnest snow

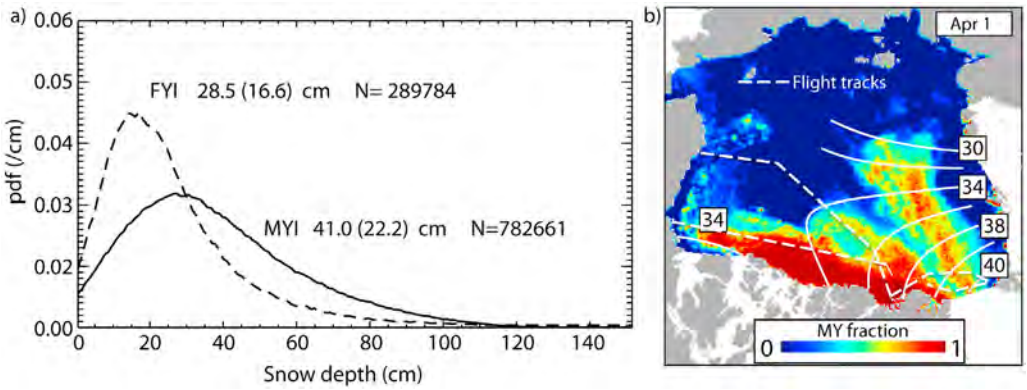

Figure 14. Snow depth on multiyear and first-year sea ice. (a) Distributions. (b) Snow depth isopleths (in cm) from climatology by *Warren et al.* [1999] overlaid on flight tracks and a map of multiyear sea ice coverage.

cover compared to the two previous flights. Snow thickness estimates are obtained in only ~24% of the radar echoes (Table 2). The mean snow depth is less than half of that from the 31 March flight. This result, together with those from earlier flights, suggests a decrease in detectability of the two interfaces as the snow cover thins.

[52] Segments 1 and 2 sampled the snow cover over seasonal ice that is <6 months old. The slight increase in snow depth around the midpoint of Segment 3 is associated with the transitioning of the ice cover into the mixture of FY and MY ice (see Figure 1). A dramatic increase in snow depth past the midpoint of Segment 4 is clearly seen in the along-track profile. From a mean thickness of ~30 cm at the 2000 km mark, the snow thickness increased to >40 cm in the short distance of ~200 km from the Lincoln Sea to the Greenland coast. This matches the mean thickness of 45 cm seen by Segment 1 of the survey on 31 March (see Figure 10) and Segment 4 on 2 April (see Figure 11). In all the distributions, there are few retrievals below 10 cm because of the detectability of the a-s interfaces and the range resolution of the system; this lower limit is discussed in section 3.

[53] The relationship between snow depth and freeboard in Figure 13d shows reasonable compatibility. Correlations between the two parameters, between 0.45 and 0.52, are within the ranges observed in the earlier flights. All segments show the characteristic plateaus in snow depth seen on previous days. At the 500 km length scale, we have not found a model to consistently describe the relationship between the two parameters. We shall return to this discussion in the conclusions. At these shallower snow depths, we do not see evidence of the plateaus, discussed above, seen in the earlier flights.

4.4. Distributions Over First-Year and Multiyear Sea Ice

[54] Figure 14a summarizes the distributions of retrieved snow depths on FY and MY ice from the three flights. To determine the ice-type membership of individual snow depth samples, we used the MYI concentrations from QuikSCAT. A snow depth estimate is classified based on its location on the low-resolution (gridded 12.5 km estimates) map: when a sample is located within a gridded cell with ≥70% MYI, it is categorized as snow depth on MY ice; samples in cells with ≤30% MYI are assigned to the FY ice category. This excludes ~40% of the samples that are in mixed MY and FY regions cells (30% < MYI fraction < 70%). Admittedly, this is a rather coarse classification, especially over the mixture of ice types in the transition zones, but it serves to summarize and contrast the snow depths collected from the three flights.

[55] The snow depth distributions on FY and MY sea ice (in Figure 14a) highlight the differences in the surveyed thicknesses from the three flight days. The mean depth is 41.0 ± 22.2 cm and 28.5 ± 16.6 cm on MY and FY sea ice, respectively. Whether these distributions are representative of the entire Arctic Ocean are subject to the caveat discussed earlier. The estimated snow depth over MY ice can be compared to the results of *Warren et al.* [1999]: their snow depth isopleths (see Figure 14b) show that the expected snow depth (on 1 April) north of Greenland and Fram Strait varies between 34 cm and 40 cm. This is within the range of what is observed here, especially the snow depths from the survey on 31 March. It is also interesting to note that the estimates from the snow radar are somewhat compatible with the sampling methodology used to construct the climatology of *Warren et al.* [1999], i.e., the samples from both data sets are representative of snow depth over relatively level MYI. However, the sampling over deformed ice remains an issue.

[56] These results are encouraging. The potential use of the retrievals for detection of interannual changes in snow depth, a proxy indicator of precipitation minus sublimation and the flux of moisture into the Arctic Ocean, over the ice cover is suggested. But, this awaits a longer time series of snow depth estimates, and in-depth comparisons with atmospheric reanalysis and the work of *Warren et al.* [1999] for vetting such acquisitions for climatological use.

5. Conclusions

[57] In this paper, we analyzed the snow radar data from three Arctic transects acquired by Operation IceBridge in 2009. Since these are the first long-range surveys of snow cover, our objectives were to examine the issues in estimating snow depth, the limitations of the current instrument, and to summarize the results of geophysical interest from these acquisitions. Here, we first summarize what we have learned in terms of radar phenomenology and snow depth retrievals before we touch on the geophysical utility of these and future snow surveys.

5.1. Snow Depth Retrievals

[58] Over relatively undeformed sea ice, the air-snow and snow-ice interfaces are clearly resolved by the ultrawideband radar and can be used to estimate snow depth. The ultimate quality of the snow depth retrievals, however, depends on not only the radar performance but also the procedure employed to detect the radar signatures of these interfaces. We implemented a simple approach to identify the location of these interfaces. To reduce the error (or false alarm) rate, the thresholds and conditions for detection are set relatively high so that only unambiguous interfaces are selected for calculation of snow depth. In consequence, weaker or less distinct air-to-snow transitions over fresh snow (low dielectric contrast) that fail to cross these detection thresholds are not selected. Results also point to a decrease in detectability of the two interfaces as the snow cover thins. In cases where the air-snow interfaces are dispersed in range, no estimates are produced because of the low signal-to-noise returns. These missing retrievals (when the interfaces are not detected by our approach) add to gaps in the radar data when the snow or ice surfaces are deformed (ridged) or sloped (not level). This represents a preferential sampling of relatively undeformed/level surfaces and a limitation of the current radar configuration. Better processing approaches more adapted to the signal characteristics of the radar are being investigated at CReSIS (S. Chakrabarti et al., A combination of nonparametric and parametric signal processing techniques for estimating snow thickness, in preparation, 2011). Finally, the finite resolution of the radar also imposes a lower limit on detectable snow thickness. For our detection algorithm, that lower limit is ~8 cm.

[59] Variability in snow density (grain size and layer structure) may be an issue in the estimation of snow depth. If we can assume that the bulk density of the snow volume is a reasonable approximation for calculation of the refractive

index, then the snow depth estimates are relatively insensitive to uncertainties of 0.1 g/cm^3. However, if the structure of the snow layer modifies the scattering significantly, then this variability may need to be considered. This would be a challenge unless these snow properties can be inferred directly from the radar data. Even though the mean backscatter of the two interfaces seems to be remarkably stable (see Figure 8); variability is probably associated with surface roughness that could be explored in the improvement of the retrieval process. Field programs can certainly provide bounds on variability, in addition to that found in the work of *Warren et al.* [1999], but the sampling requirements can be challenging.

[60] The trans-Arctic radar surveys from OIB provided along-track profiles for examining regional variability and gradients in snow depths in the transition from a purely seasonal to MYI cover. The thickest snow, at 48 cm (mean over 500 km segments), is found in the Fram Strait region. This region has the thickest snow cover in the Arctic Ocean, not just because of the older ice, but it is also situated in the path of storm tracks entering the Arctic Ocean. The thinnest snow (~22 cm) is found north of Barrow. Examination of the retrievals in conjunction with maps of seasonal and MYI coverage show dependence of snow depth on ice age. Near the beginning of April, mean snow depths are 28.5 ± 16.6 cm and 41.0 ± 22.2 cm over the first-year and MYI surveyed by the snow radar. Snow depth over MYI is comparable to the climatology of W99. Snow depth is thinner over the large expanse of seasonal ice in the Beaufort Sea but gets progressively thicker toward the MYI cover north of Ellesmere Island, Greenland and the Fram Strait. Correlations between freeboard and snow depth (over level ice) are moderate; we have not found a model to consistently describe the relationship between the two parameters. Presumably, over level ice, they should be dependent on local ice age as well as local snow accumulation.

5.2. Utility of Snow Depth

[61] Of immediate geophysical interest is the use of these estimates to understand the spatial distribution of snow depth over sea ice and for improvements of satellite retrievals of sea ice thickness. Repeated annual trans-Arctic surveys performed around the same time of year can provide sufficient data to paint a broad picture for depicting regional and interannual variability, and perhaps estimating trends in snow depth. For this type of usage, consistent retrievals are crucial, i.e., controlling the radar configuration as well as the detection algorithms. Even though Operation IceBridge will last till the launch of ICESat 2 in 2016, establishing a true monitoring capability is a challenge since this is the first time where this type of survey is available. At finer length scales, unless the sampling issues over deformed ice discussed earlier can be resolved, the use of snow depth retrievals, for comparisons with models and understanding of snow depth related processes (e.g., surface heat balance), maybe somewhat limited.

[62] As for contributions to cryospheric remote sensing, the most important application will be to understand snow loading for estimation of ice thickness [*Kwok*, 2011]. To obtain sea ice thickness, current and planned satellite altimeters provide only sea ice freeboard (radar) or the combined snow and ice freeboard (lidar). Snow loading has been left as an estimate to be obtained elsewhere. However, routine measurements of snow depth and density over the Arctic Ocean are not available. One could utilize the snow climatology of the Arctic Ocean sea ice cover [*Warren et al.*, 1999] but this was compiled over relatively level MYI, and this has not been updated since 1991. Airborne surveys of snow depth, even though spatially and temporally limited, could potentially contribute to the understanding of the following:

[63] 1. The best source of measurements to provide the snow depth estimates for use in freeboard-based thickness estimation. The radar snow depths could be used as an assessment reference.

[64] 2. The variability of snow depths over length scales shorter than that produced by meteorological models.

[65] 3. The best approach for partitioning estimates of mean snow depth from a larger/coarser length scale (100 km) into the higher-resolution distributions used by radar and lidar altimetry [*Kwok and Cunningham*, 2008]. Also, the relationship between snow depth and freeboard at different length scales.

[66] 4. The biases due to partial penetration into the snow volume in radar freeboard retrievals. There could be biases in the estimated freeboard if the returns were not directly from the snow-ice interface.

[67] 5. The uncertainties in snow depth estimates derived from satellite passive microwave measurements [*Markus and Cavalieri*, 1998].

[68] In sum, the snow radar retrievals will be useful in a number of contexts. We have examined only a small facet of this rich data set. No doubt there will be other applications once the retrievals become generally available. We see that the multiyear data collections will be useful in geophysical applications as well as developing and improving the observational technology. The radar performance has and will be improved with each OIB deployment: these improvements will allow the detection of weaker interfaces and will reduce the limitations due to deformed ice.

[69] **Acknowledgments.** The QuikSCAT data are provided by the Physical Oceanography DAAC at the Jet Propulsion Laboratory, Pasadena, California. The IceBridge snow radar data are provided by the National Snow and Ice Data Center. The snow radar development was carried out by CReSIS with support from NASA and NSF. R.K., S.P., and B.H. carried out this work at the Jet Propulsion Laboratory, California Institute of Technology, under contract with the National Aeronautics and Space Administration.

References

Cavalieri, D. J., and T. Markus (2006), EOS Aqua AMSR-E Arctic sea-ice validation program: Arctic2006 aircraft campaign flight report, *NASA Tech. Memo.*, *TM-2006-214142*, NASA Goddard Space Flight Cent., Greenbelt, Md.

Giles, K. A., et al. (2007), Combined airborne laser and radar altimeter measurements over the Fram Strait in May 2002, *Remote Sens. Environ.*, *111*(2–3), 182–194, doi:10.1016/j.rse.2007.02.037.

Kanagaratnam, P., T. Markus, V. Lytle, B. Harvey, P. Jansen, G. Prescott, and P. Gogenini (2007), Ultrawideband radar measurements of thickness of snow over sea ice, *IEEE Trans. Geosci. Remote Sens.*, *45*(9), doi:10.1109/TGRS.2007.900673.

Krabill, W. B., et al. (2002), Aircraft laser altimetry measurement of elevation changes of the Greenland ice sheet: Technique and accuracy assessment, *J. Geodyn.*, *34*, 357–376, doi:10.1016/S0264-3707(02)00040-6.

Kwok, R. (2004), Annual cycles of multiyear sea ice coverage of the Arctic Ocean: 1999–2003, *J. Geophys. Res.*, *109*, C11004, doi:10.1029/2003JC002238.

Kwok, R. (2011), Satellite remote sensing of sea ice thickness and kinematics: A review, *J. Glaciol.*, *56*(200), 1129–1140, doi:10.3189/002214311796406167.

Kwok, R., and G. F. Cunningham (2008), ICESat over Arctic sea ice: Estimation of snow depth and ice thickness, *J. Geophys. Res.*, *113*, C08010, doi:10.1029/2008JC004753.

Kwok, R., G. F. Cunningham, M. Wensnahan, I. Rigor, H. J. Zwally, and D. Yi (2009), Thinning and volume loss of Arctic sea ice: 2003–2008, *J. Geophys. Res.*, *114*, C07005, doi:10.1029/2009JC005312.

Markus, T., and D. J. Cavalieri (1998), Snow depth distribution over sea ice in the Southern Ocean from satellite passive microwave data, in *Antarctic Sea Ice: Physical Processes, Interactions and Variability*, *Antarct. Res. Ser.*, vol. 74, edited by M. O. Jeffries, pp. 19–39, AGU, Washington, D. C.

Markus, T., J. C. Stroeve, and J. Miller (2009), Recent changes in Arctic sea ice melt onset, freezeup, and melt season length, *J. Geophys. Res.*, *114*, C12024, doi:10.1029/2009JC005436.

Panzer, B., C. Leuschen, A. Patel, T. Markus, and S. Gogineni (2010), Ultrawideband radar measurements of thickness of snow over sea ice, *IEEE Trans. Geosci. Remote Sens.*, *45*, 2715–2724, doi:10.1109/IGARSS.2010.5654342.

Patel, A. (2009), Signal generation for FMCW ultrawideband radar, M.S. thesis, Dep. of Electr. Eng. and Comput. Sci., Univ. of Kansas, Lawrence.

Sturm, M., J. Holmgren, and D. K. Perovich (2002), Winter snow cover on the sea ice of the Arctic Ocean at the Surface Heat Budget of the Arctic Ocean (SHEBA): Temporal evolution and spatial variability, *J. Geophys. Res.*, *107*(C10), 8047, doi:10.1029/2000JC000400.

Sturm, M., J. A. Maslanik, D. K. Perovich, J. C. Stroeve, J. Richter-Menge, T. Markus, J. Holmgren, J. F. Heinrichs, and K. Tape (2006), Snow depth and ice thickness measurements from the Beaufort and Chukchi seas collected during AMSR-Ice03 Campaign, *IEEE Trans. Geosci. Remote Sens.*, *44*(11), 3009–3020, doi:10.1109/TGRS.2006.878236.

Ulaby, F. T., R. K. Moore, and A. K. Fung (1986), *Microwave Remote Sensing*, vol. 3, *From Theory to Applications: Active and Passive*, Artech House, Norwood, Mass.

Warren, S. G., I. G. Rigor, N. Untersteiner, V. F. Radionov, N. N. Bryazgin, Y. I. Aleksandrov, and R. Colony (1999), Snow depth on Arctic sea ice, *J. Clim.*, *12*(6), 1814–1829.

Wilyard, R. (2006), Airborne radar for measuring snow thickness over sea ice, *CReSIS Tech. Rep. 108*, 90 pp., Univ. of Kansas, Lawrence.

S. Gogineni, C. Leuschen, and B. Panzer, Center for Remote Sensing of Ice Sheets, University of Kansas, 2335 Irving Hill Rd., Lawrence, KS 66046, USA.

B. Holt, R. Kwok, and S. Pang, Jet Propulsion Laboratory, California Institute of Technology, 4800 Oak Grove Dr., Pasadena, CA 91109, USA. (ron.kowk@jpl.nasa.gov)

T. Markus, NASA Goddard Space Flight Center, Greenbelt, MD 27701, USA.